ACS NANO

www.acsnano.org

ARTICLE

Strain-Induced Indirect-to-Direct Bandgap Transition, Photoluminescence Enhancement, and Linewidth Reduction in Bilayer $MoTe_2$

Yueyang Yu, Chuan-Ding Dong, Rolf Binder,* Stefan Schumacher,* and Cun-Zheng Ning*

Cite This: *ACS Nano* 2023, 17, 4230−4238

Read Online

ACCESS | Metrics & More | Article Recommendations | Supporting Information

ABSTRACT: Two-dimensional (2D) layered materials provide an ideal platform for engineering electronic and optical properties through strain control because of their extremely high mechanical elasticity and sensitive dependence of material properties on mechanical strain. In this paper, a combined experimental and theoretical effort is made to investigate the effects of mechanical strain on various spectral features of bilayer $MoTe_2$ photoluminescence (PL). We found that bilayer $MoTe_2$ can be converted from an indirect to a direct bandgap material through strain engineering, resulting in a photoluminescence enhancement by a factor of 2.24. Over 90% of the PL comes from photons emitted by the direct excitons at the maximum strain applied. Importantly, we show that strain effects lead to a reduction of the overall linewidth of PL by as much as 36.6%. We attribute the dramatic decrease of linewidth to a strain-induced complex interplay among various excitonic varieties such as direct bright excitons, trions, and indirect excitons. Our experimental results on direct and indirect exciton emission features are explained by theoretical exciton energies that are based on first-principles electronic band structure calculations. The consistent theory-experimental trend shows that the enhancement of PL and the reduction of linewidth are the consequences of the increasing direct exciton contribution with the increase of strain. Our results demonstrate that strain engineering can lead to a PL quality of the bilayer $MoTe_2$ comparable to that of the monolayer counterpart. The additional benefit of a longer emission wavelength makes the bilayer $MoTe_2$ more suitable for silicon-photonics integration due to the reduced silicon absorption.

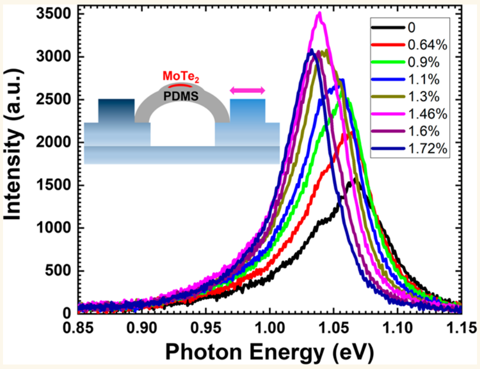

KEYWORDS: *2D materials, molybdenum ditelluride, strain effects, photoluminescence enhancement, linewidth reduction*

Layered transition metal dichalcogenides (TMDCs) have been widely studied for their potential application in photonic devices.[1,2] One of the advantages of TMDCs has been their layer-number-dependent bandgaps which lead to optical emission covering a large spectral range.[3,4] However, most TMDCs are indirect bandgap materials for the thickness of more than a monolayer.[3] Such indirect bandgap multilayer TMDCs have a low quantum yield and are poorly suited for applications in optoelectronic devices. Among all TMDCs, $MoTe_2$ has been especially interesting as one of the very few monolayer materials that emit in the near-infrared with photon energy slightly below the silicon absorption edge, suitable for silicon-based integrated photonics. For many applications, emission of longer wavelengths than that of monolayer $MoTe_2$ would be desirable both to cover a different wavelength band and to be further away from the silicon absorption edge to reduce the absorption. In this sense, a bilayer $MoTe_2$ with a direct bandgap would be ideal with less absorption.

Strain engineering has been applied on various layered TMDCs to modify their optical properties experimentally.[5−13] Since many monolayer TMDCs are direct gap semiconductors, strain engineering typically degrades their PL qualities, leading to decreased intensities and increased linewidths due to the direct-to-indirect bandgap transition.[5−12] Among all TMDCs, a strain-induced indirect-to-direct bandgap transition has only been reported on bilayer WSe_2 so far.[13] For bilayer WSe_2, the difference between the indirect and direct gap is around 40 meV, making the crossover possible with achievable strain values. Bilayer $MoTe_2$ shares a similarly small energy difference

Received: February 17, 2022
Accepted: February 6, 2023
Published: February 22, 2023

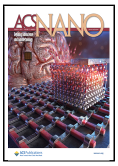

https://doi.org/10.1021/acsnano.2c01665

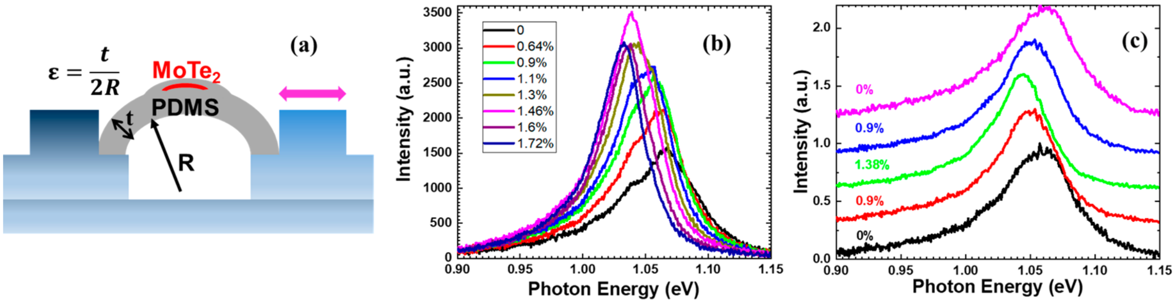

Figure 1. (a) Schematic of the setup used for applying strain to MoTe$_2$. (b) Photoluminescence spectra of bilayer MoTe$_2$ under different levels of tensile strain. (c) Normalized PL spectra (offset for clarity) for successive levels of strain from 0%, 0.9%, 1.38%, 0.9%, and 0% to test the reversibility of the strain effects.

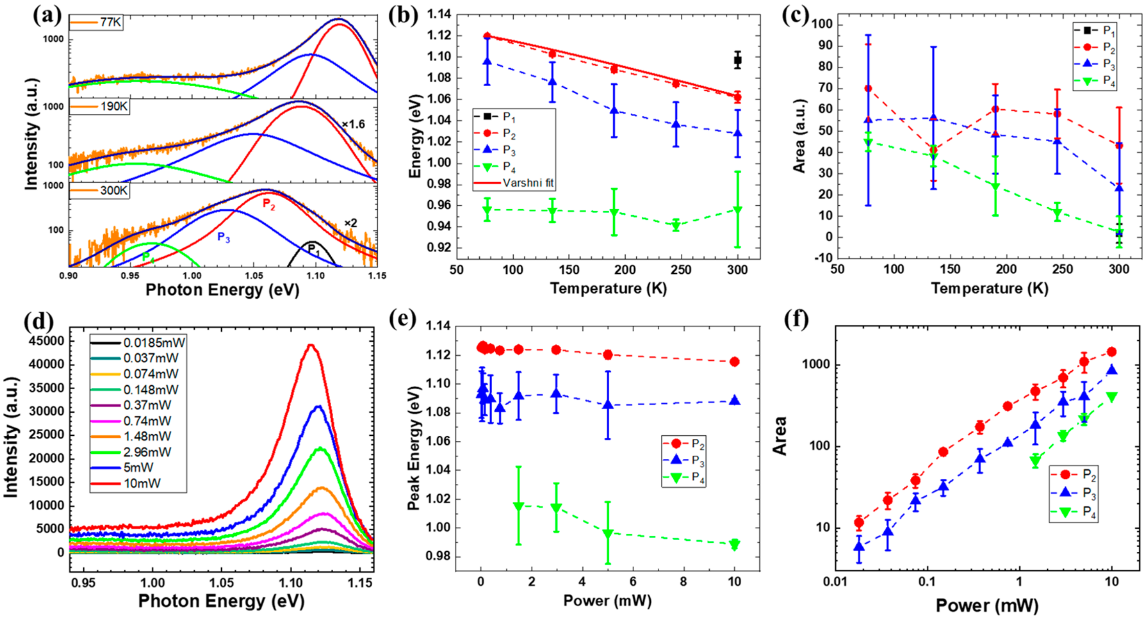

Figure 2. (a) PL spectra of bilayer MoTe$_2$ without strain at 77 K, 190 K, and 300 K fitted with multiple Voigt peaks. (b) Peak energies vs temperature. The energies of Peak 2 are fitted by the Varshni equation. (c) Integrated peak intensities of Peaks 1−4 vs temperature. (d) PL spectra of unstrained bilayer MoTe$_2$ at different pumping levels at 77 K. (e) Peak energies of Peaks 2−4 vs pumping power extracted from (d). (f) Light-out-light-in (L-L) curve: Integrated peak intensities of Peaks 2−4 extracted from (d). The error bars in (b), (c), (e), and (f) represent one standard deviation in the least-squares fits, details of which can be found in the Supporting Information Section 1.

between the indirect and direct gaps. It is estimated to be around 60 meV by a theoretical calculation,[14] much smaller than in other bilayer TMDCs.[15−17] It was also theoretically predicted that bilayer MoTe$_2$ can be converted into a direct bandgap semiconductor under an isotropic tensile strain of 1% in three dimensions.[18] All this indicates that bilayer MoTe$_2$ is an ideal candidate for potentially changing from indirect to direct bandgap through strain engineering, leading to further increase of PL yield. In this work, we experimentally demonstrate simultaneous PL enhancement and linewidth reduction on bilayer MoTe$_2$ by applying uniaxial tensile strain, showing strong signatures of transition from an indirect to a direct bandgap material. Through theoretical calculations specifically incorporating the uniaxial strain features of our experiments, we were able to discover the interplay between different exciton species during the process of transition from indirect to direct bandgap.

RESULTS AND DISCUSSION

Experimental Results. The customized setup used to apply strain on MoTe$_2$ is schematically shown in Figure 1a. The polydimethylsiloxane (PDMS) substrate is bent by fixing one end and pressing the other end by a moving block. Uniaxial tensile strain is transferred onto the sample from the PDMS. Its value is estimated as $\varepsilon = t/2R$, where t is the thickness of the PDMS and R is the radius of curvature. For the preparation of PDMS and the discussion of strain transfer, see Methods and Supporting Information Section 9, respectively.

In situ PL measurement is performed as strain is applied on the samples. Figure 1b shows the PL spectra of bilayer MoTe$_2$ at different strain levels up to 1.72%. There are several direct observations as strain is increased. The PL peak red-shifts along with the increase of PL intensity as strain is increased. The maximum red-shift is around 34.8 meV in the range of strain applied with the PL peak intensity increasing by a factor of ~2.24. Additionally, we observe a reduction in the spectral linewidth. These features will be more systematically studied later on (see Figure 5d), together with the discussions of the physical origins of these changes. We also tested the reversibility of the strain effects by applying and releasing the strain. The normalized PL spectra during this process are shown in Figure 1c, where we can see a fully restored spectrum

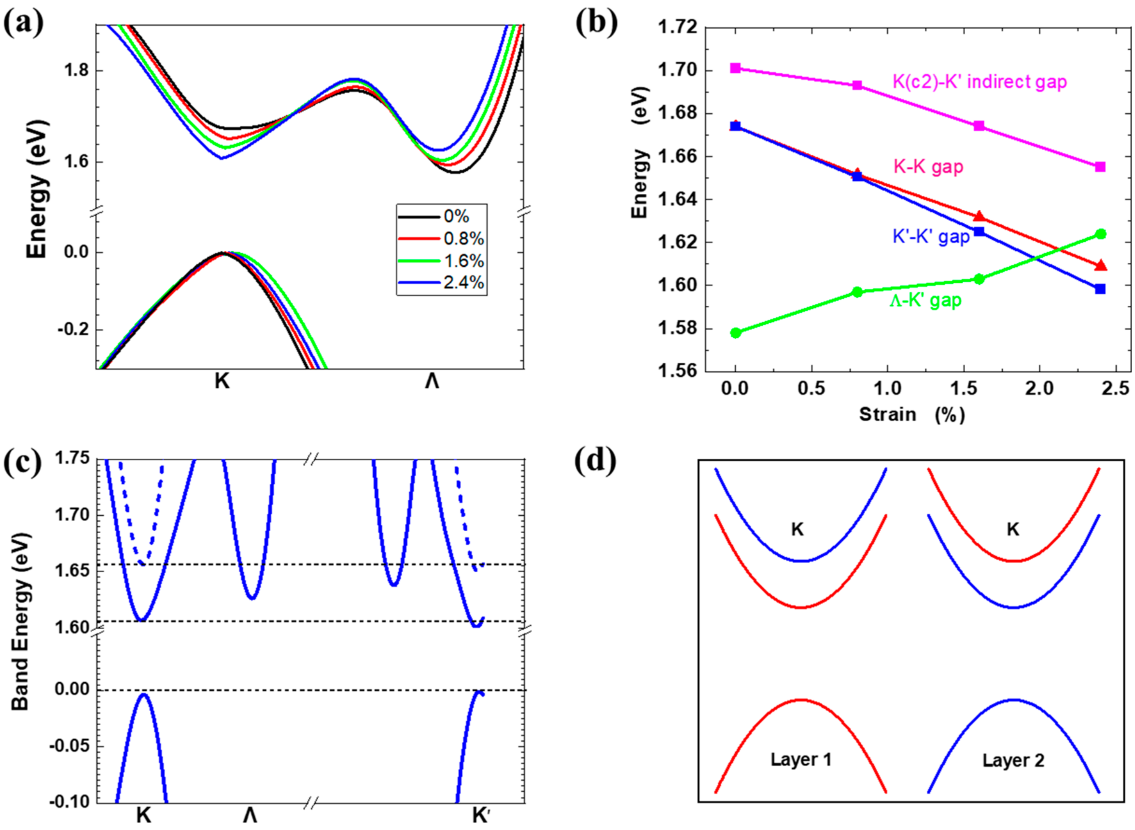

Figure 3. Theoretical calculation of band structures. (a) Electronic band structure for bilayer $MoTe_2$ at 0%, 0.8%, 1.6%, and 2.4% strain using DFT+GW calculations. Only the highest valence band and the lowest conduction band at K and Λ valleys are shown here for simplicity. (b) Bandgap energies for different transitions of bilayer $MoTe_2$. (c) Electronic band structure at selected k-points for bilayer $MoTe_2$ at 2.4% strain; dashed lines represent the second-lowest conduction band. (d) Schematic diagram of the band structures in the K valley. Energy states with the same spin are plotted in the same color.

after strain is released. Based on the steady improvement of the PL quality with strain and the complete reversibility of spectral features, the material seems to be free from mechanical damage or slippage with respect to the substrate after up to 1.38% strain is applied, indicating full reversibility of the strain effects within this range. Effects of wrinkles, cracks, and other inhomogeneities can also be reasonably excluded in the PL spectra we show in this work, since the spot size of the pumping laser is only 1 μm in diameter. And we have not seen significant variations of spectral features in our measurements of many different samples without strain. More importantly, the reversibility of the spectrum mentioned above seems to be inconsistent with the existence of wrinkles and cracks.

To identify the spectral features of PL of bilayer $MoTe_2$, temperature-dependent PL measurements without applying strain were conducted. PL spectra were recorded at different temperatures down to 77 K, as shown in Figure 2a in log scale. The spectra are fitted by up to 4 peaks P_1 through P_4, each having a Voigt line shape which is the convolution of a Lorentzian with a Gaussian function. The temperature-dependent peak energies and areas are plotted in Figure 2b and Figure 2c, respectively. At room temperature, P_1 has the highest peak energy. As the temperature is decreased, P_1 is no longer visible in the PL spectra. We leave Peak 1 for further discussion due to its limited data points in the temperature-dependent PL measurements. The energy of P_2 is 1.062 eV at room temperature, close to the A exciton energy (1.07 eV) in ref 19. Consistent with previous studies,[20,21] we identify the highest peak P_2 as the neutral exciton emission, originating from the direct transitions in the K or K′ valley. The P_2 energies increase as temperature decreases as a result of thermal contraction. They are fitted by the Varshni equation[22] $E_g(T) = E_g(0) - \frac{\alpha T^2}{T+\beta}$, which is typically used to describe the temperature dependence of semiconductor bandgaps. We obtain $E_g(0) = 1.13$ eV, $\alpha = 2.95 \times 10^{-4}$ eV/K, and $\beta = 100$ K. We notice our parameters are slightly different from the ones obtained by Helmrich et al.[21] Such difference is believed to be a result of the different substrates used. In our case, the PDMS has a different thermal expansion coefficient from SiO_2. And the bilayer $MoTe_2$ could slide with respect to PDMS. Consequently, the peaks do not shift as much when the temperature is decreased. We conduct pump power-dependent PL measurements at 77 K. The laser power at the sample is increased from 18.5 μW up to 10 mW. The corresponding PL spectra are shown in Figure 2d. Multiple Gaussian peaks are used to fit the spectra. Fitting details can be found in the Supporting Information (Figure S1). The pump power-dependent peak energies and areas are plotted in Figure 2e and 2f, respectively. As is shown in Figure 2e, the energy of P_2 decreases by 10 meV as excitation density increases. Such a red-shift can be explained by a combined effect of bandgap renormalization and plasma screening.[23] The light-out-light-in (L-L) curve of the neutral exciton (P_2) in Figure 2f has the largest slope of 0.9 in the low pumping regime, close to 1, which is the slope for typical neutral exciton emissions. At pumping power higher than 0.74 mW, the curves become

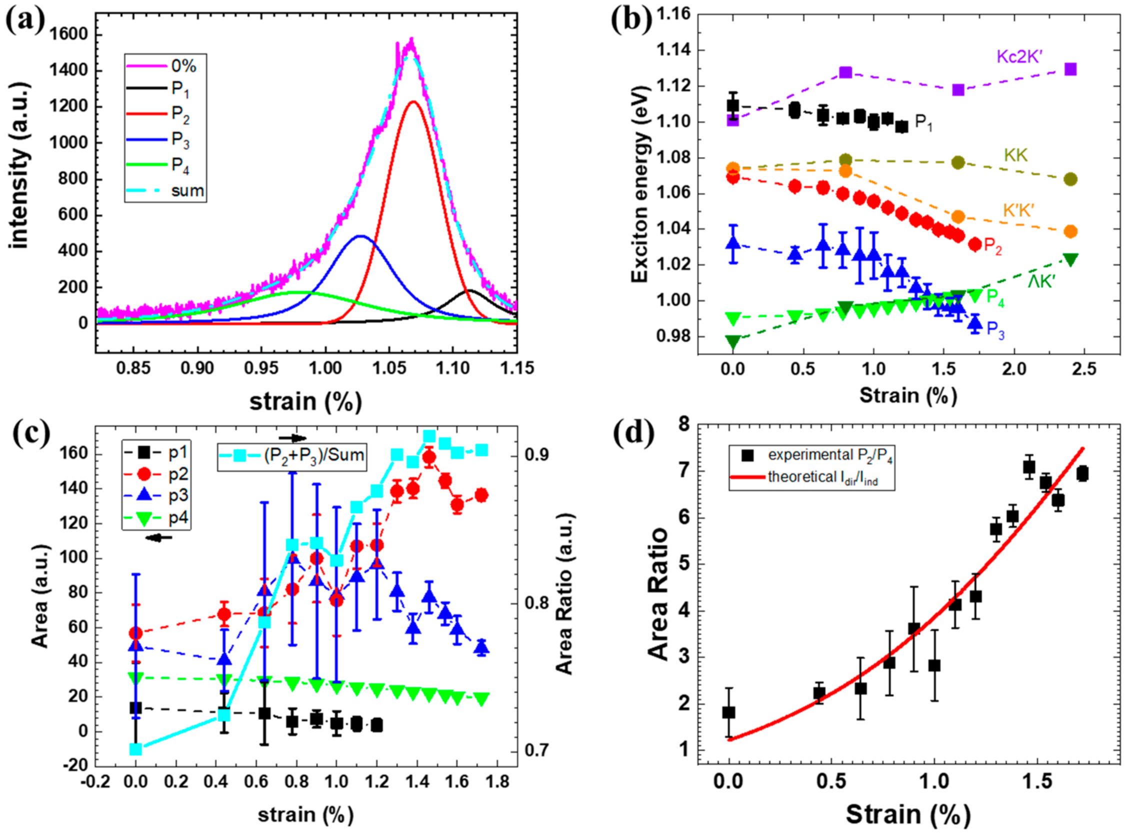

Figure 4. Strain-dependent spectral features: (a) PL spectra of bilayer $MoTe_2$ at room temperature fitted with multiple Voigt peaks at 0% strain. (b) Strain dependence of the peak energies of Peaks 1−4 and the theoretically estimated energies of different excitonic species. (c) Left *y* axis: Integrated intensity of each peak vs strain. Right *y* axis: Ratio of the direct transition (P_2+P_3) over the total emission. (d) Experimental peak area ratio P_2/P_4 (black squares) and fitting (red line) to the expression of I_{dir}/I_{ind} in eq 1 to determine the coefficients *a* and *b*. The error bars in (b), (c), (d) represent one standard deviation in the least-squares fits.

sublinear, likely due to other nonlinear processes such as biexciton formation or exciton−exciton annihilation, which is beyond the scope of this work.

Peak 3 (P_3) is centered at 1.028 eV at room temperature, 35 meV lower than P_2. It is not resolved as a separate peak at room temperature in previous studies.[20,24] Its energies have a similar increasing trend as P_2 when temperature decreases, as shown in Figure 2b. Its peak energy and intensity follow the same trend as P_2 when pumping increases, as shown in Figure 2e and 2f. This suggests that the origin of P_3 is similar to that of P_2 or related to the direct transition in the K (K′) valley. We attribute P_3 to the trion emission, consistent with the trion binding energy of 24−27 meV measured in monolayer $MoTe_2$.[25] The trion binding energy in bilayer $MoTe_2$ decreases from 35 meV at RT to 20.5 meV at 77 K based on our measurement. As temperature decreases, trion emission is enhanced in Figure 2c, as a result of fewer trions ionized by the decreasing thermal energy.

Finally, we look at the lowest energy peak, Peak 4 (P_4). It centers around 0.96 eV at room temperature and becomes more pronounced as the temperature decreases. It has a very broad peak with a FWHM of 214 meV at 77 K. And the slope of the L-L curve in Figure 2f is 0.813. With these observations, we tentatively assign it as the phonon-assisted indirect transition from Λ_C-K_V corresponding to an indirect exciton. The indirect exciton emission increases with a decrease in temperature. In general, the PL due to indirect exciton recombination is determined by exciton and phonon population factors. Even though the phonon-assisted transitions comprise emission and absorption of phonons, the phonon emission dominates at low temperatures and hardly changes with the thermal populations. In that case, the temperature dependence of the PL is dominated by the exciton population factors. To this end, a detailed theoretical analysis is given in ref 26, which also motivated our use of the fit formula, eq 1, for the area ratio of direct (P_2) to indirect (P_4) exciton emissions in Figure 4d. As shown by our theoretical calculations (details in the next section), the Λ-K bandgap is the smallest bandgap for bilayer $MoTe_2$. In addition, the Λ-K excitons are increasingly populated with decreasing temperature. These features agree with what is expected from the indirect Λ_C-K_V transition.

Theoretical Results. To more quantitatively understand the strain-induced changes in PL spectra, band structure calculations of the bilayer $MoTe_2$ were performed. Selected electronic bands of unstrained and strained bilayers of $MoTe_2$ are compared in Figure 3a, while plots of the more comprehensive band structure are given in the Supporting Information (Figure S3). The valence band has its maximum value at K and K′ points with or without strain. K and K′ are degenerate in energy without strain. When no strain is applied, the conduction band has its minimum at the Λ point, indicating bilayer $MoTe_2$ is an indirect bandgap material, consistent with other calculations in the literature.[27] As strain is applied, we see that the conduction band minimum at K and K′ decreases, accompanied by the increase of the minimum at

Λ with the increase of strain levels. In other words, strain makes the bandgap of bilayer $MoTe_2$ more direct. Transition energies at selective k-points are extracted and plotted in Figure 3b. At 0% strain, the indirect transition from Λ in the conduction band to K′ in the valence band (green line) has the lowest energy of 1.578 eV. Direct transition at the K or K′ valley (red/blue lines) has a value of 1.674 eV, leading to a Λ-K difference of ∼96 meV, among the smallest for bilayer TMDCs.[15−17] As strain is increased, the Λ-K′ gap increases while both the K-K and K′-K′ gaps decrease. The Λ-K′ gap and K′-K′ gap cross over at strain values of approximately 2%, theoretically indicating a strain-induced indirect−direct bandgap transition in bilayer $MoTe_2$. The maximum strain (1.72%) in our experiment is quite close to the theoretical transition point.

Figure 3c shows the band structure in the larger range of wavevector at 2.4% strain with also the inclusion of the split-off conduction band due to spin−orbital coupling (SOC). We see a clear lifting of degeneracy between K and K′ due to the strain-induced symmetry breaking. Both of the conduction band edges are lower at K′ than at K, while the top of the valence band is slightly higher at K′ than at K. As a result, the bandgap is smaller (by 10 meV) at K′. The degeneracy of the K and K′ valleys has been lifted by the uniaxial strain.[28,29] Such a lifting of the K−K′ degeneracy could lead to a preferential occupation of the K′ valley, leading potentially to steady-state valley polarization, especially at higher strain levels with larger K-K′ splitting.

Analysis Based on Experiment-Theory Comparison. So far, Peak 2 has been attributed to the neutral exciton emission, Peak 3 to the trion emission, and Peak 4 to the indirect exciton emission, based on the discussion in the Experiment Results section. We also like to further discuss the origin of P_1 in Figure 2. In bilayer TMDCs with AB stacking, both spin and valley are coupled to the layer pseudospin.[30] In a given valley, the spin configuration is locked to the layer index. We show the widely adopted schematic spin polarized band structures in Figure 3d. States with the same spin are plotted in the same color. Contrary to WSe_2, in Mo-based TMDCs, the upper conduction band (CB2) in layer 2 has the same spin states with the highest valence band in layer 1 (see Figure 3d). With interlayer hopping, holes in layer 2 can form a bright exciton with electrons in CB2 in layer 1. Such spatially indirect excitons have been reported in other multilayer TMDCs like MoS_2,[31−33] $MoSe_2$,[34] WSe_2[35] and heterobilayers.[36,37] But so far they have not been observed in any room temperature PL spectra, likely due to the low quantum efficiency in those indirect gap multilayer TMDCs. In bilayer $MoTe_2$, the energy separation (ΔE_1) between the two lowest conduction bands at the K valley is 27 meV at 0 strain, close to the separation (33.9 meV) we see between P_1 and P_2 in Figure 2b. This suggests the association of P_1 with the interlayer exciton emission, whose energy should be higher than the intralayer K_C-K_V exciton (P_2), as shown in Figure 3d. The near degeneracy of Λ and K in bilayer $MoTe_2$ results in more direct transitions in the K valley, compared to other TMDCs. This would also explain the fact that P_1 only exists in RT spectra. As temperature decreases, the interlayer indirect excitons are less populated. Theoretically, P_1 can also originate from K_{C2}-K'_V transitions, like the momentum-dark excitons observed in monolayer[26] and bilayer[38] WSe_2. The intervalley transition requires emission or absorption of a phonon for conservation of energy and momentum. In this paper, we do not have enough evidence to completely rule out this possibility, but we consider that the interlayer exciton, which involves only intravalley recombination, is more likely the case here.

Similar to the multipeak Voigt fittings in Figure 2a, PL spectra at varying levels of strain at room temperature are fitted. An example of such fitting is shown in Figure 4a at 0% strain. Corresponding peaks for the rest of the strain levels and discussion about different fitting methods can be found in the Supporting Information Section 4.

The strain dependence of the peak energies for the four peaks is shown in Figure 4b together with the theoretical energies of the $K_{C2}K'$, KK, K′K′, and ΛK′ excitons (in this notation, the first state refers to the conduction band and the second to the valence band; e.g., ΛK′ refers to the transition from the lowest conduction band at Λ to the highest valence band at K′). In order to compute the exciton energies, we solve the Wannier equation for TMDCs within a 2-band model for hyperbolic bands with various mass parameters. For a given strain, we then associate the band structure obtained from the first-principles calculation with the hyperbolic band that approximately reproduces the first-principles calculation band structure, and thus we obtain an estimate for the exciton energy from the combination of the first-principles band structure and the solution of the Wannier equation. More details are given in Section 5 of the Supporting Information.

From Figure 4b we see that, without strain, P_1 corresponds to the theoretical $K_{C2}K'$ exciton with a difference of 8 meV. We see that the peak energy of P_1 slowly decreases with strain while that of $K_{C2}K'$ fluctuates around 1.11 eV. This deviation can result from the error in the estimation of the exciton binding energy or uncertainty in the fitting of P_1, given it is the weakest emission, especially at high strain levels. At zero strain, P_2 corresponds to the KK or K′K′ exciton (both are degenerate at zero strain) with a difference of only 5 meV. P_2 and P_3 both red-shift at the same rate (∼ −28 meV/%) as strain increases, as a result of the shrinking K-K and K′-K′ gap. This further verifies that P_2 corresponds to the neutral-exciton emission within the K or K′ valley, while P_3 corresponds to the associated trion emission, whose theoretical energy is not included in the calculation. After including the binding energy, we see a larger split between the KK and K′K′ exciton energies (30 meV) at 2.4% strain compared to their bandgap difference (10 meV). The trend of P_2 compares well with the theoretical value of the K′K′ exciton within 0−1.6%. This indicates that at zero and small strain values, P_2 contains both KK and K′K′ excitons. And as strain increases, the more populated K′ valley makes the K′K′ exciton emission dominate in P_2. We cannot rule out the possibility that the KK exciton emission is partially merged into P_1 at higher strain levels. Finally, P_4 corresponds to the ΛK′ exciton with a difference of 13 meV at 0 strain. The trend of the theoretical ΛK′ exciton matches well with that of P_4. This again verifies the assignment of P_4 in the previous discussion about Figure 3b. We notice that the theoretical exciton energies for ΛK′ and K′K′ do not cross before the strain level of 2.4%, as opposed to their bandgap energies which cross before 2% strain (see Figure 3b). The experimental data show that the energy of P_4 is always lower than that of P_2. But it is clear from Figure 4b that both the theoretical and experimental results show the same consistent trend of indirect to direct transition. Our data shows that the maximum strain achieved in our experiment is very close to the theoretical indirect−direct transition point.

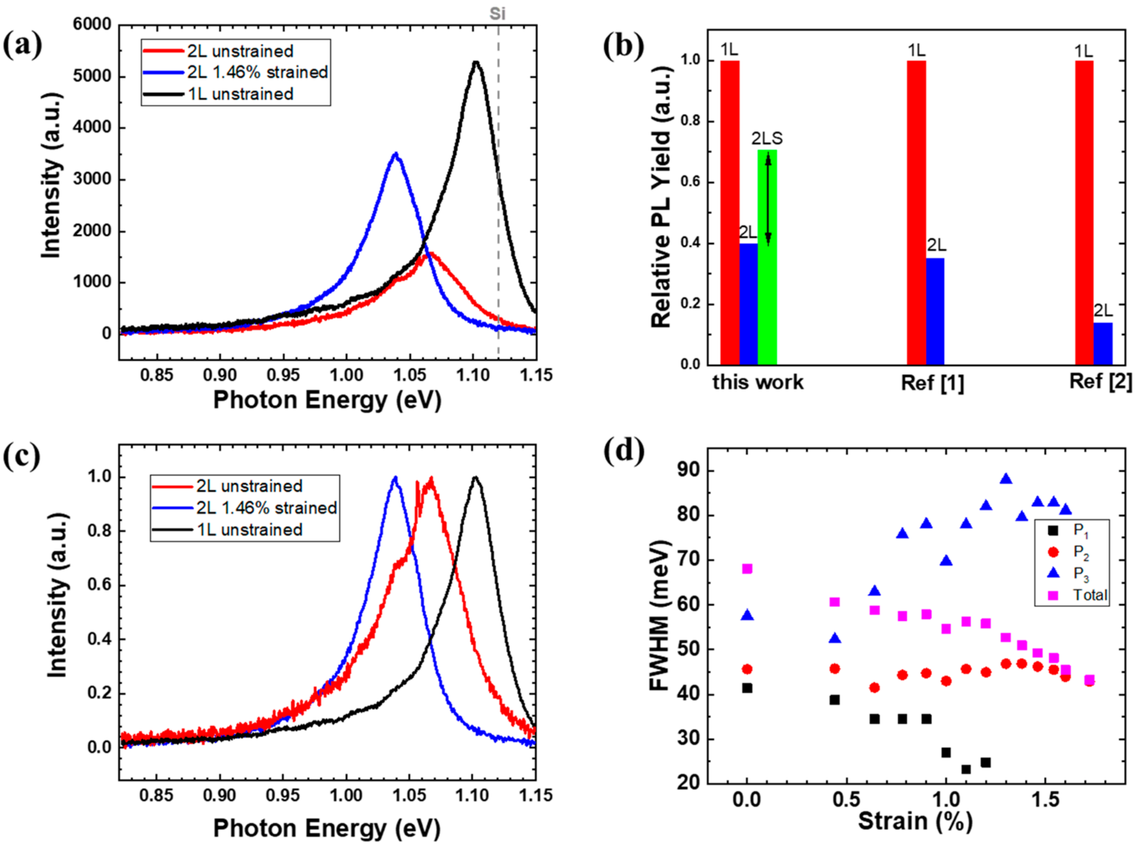

Figure 5. (a) PL spectra of the unstrained bilayer, strained bilayer, and unstrained monolayer $MoTe_2$. (b) Comparison of PL yield between monolayer and bilayer $MoTe_2$ from this work and the literature.[14,19] (c) Normalized spectra in (a). (d) Resolved peak (with aforementioned peak assignment) linewidths (FWHM) and the full linewidth vs strain.

Figure 4c shows the integrated intensities of the four peaks as a function of the strain. We see that P_2 shows the most pronounced and almost monotonic increase with strain among all three peaks and is the main reason for the increase in the total PL intensity. This is consistent with the trend of the theoretical prediction of the indirect−direct band gap transition. As can be inferred from Figure 3a and 3c, the exciton population of the K′ valley increases at the expense of the Λ valley population as strain increases, leading to more K′K′ exciton population. Both direct exciton densities and recombination rate increase as strain modifies the band structure of the bilayer $MoTe_2$. Notably, the trion emission intensity reaches its maximum around the strain of 0.74%. This is reasonable as trions require the existence of excess electrons or holes which are limited as the bilayer $MoTe_2$ is sealed in PDMS. We also plot the ratio of the direct transition (P_2+P_3) to the overall emission in Figure 4c. This ratio increases from 0.7 to over 0.9 as strain increases. The tensile strain has almost changed the bilayer $MoTe_2$ to a direct gap material with 90% of the emission coming from the direct transitions. This again verifies that the maximum strain value achieved here is very close to the required strain level for the indirect to direct transition. Above 1.5% of strain, both the exciton emission and total emission decrease with strain. Finally, we see that the intensity of P_1 gradually decreases with strain, and P_1 disappears at 1.2%. This can be explained by the increasing energy separation between P_1 and P_2, as predicted by the theoretical energy difference (ΔE_1) of the two conduction bands (see Figure 3b) at K as well. A detailed comparison of the experimental peak area ration P_1/P_2 and its theoretical value can be found in the Supporting Information (Figure S8).

It is worth noting that the maximal strain value achievable in our experiment was limited by the mechanical setup. We found that the spectral peaks stopped shifting for strain levels beyond 1.72%. This could be due to slippage of the $MoTe_2$ against the PDMS layers after a certain level of strain. As we pointed out, over 90% of the PL is already from the emission of the direct excitons under the current maximal strain applied. With better PDMS or other methods to improve the adhesiveness between $MoTe_2$ and the PDMS, we believe the overall transition to a direct bandgap could be further improved.

To further verify our peak assignment and to confirm the indirect-to-direct transition, we compare the PL intensity ratio of direct (P_2) to indirect (P_4) exciton emissions in Figure 4d. The experimental area ratio obtained from Figure 4c is compared with the fit formula

$$\frac{I_{\text{dir}}}{I_{\text{ind}}} = \frac{1}{a + b\exp\left(\frac{\Delta E}{kBT}\right)} \tag{1}$$

Here ΔE is the energy difference between K′K′ and ΛK′ excitons as given in Figure 4b. This fit formula is motivated by the microscopic theory of indirect-exciton photoluminescence given as eqs 2 and 3 in ref 26, assuming that all sums in those equations contain only one state and that the phonon frequency is much smaller than the energetic difference between direct and indirect excitons. The value for ΔE (eV) = $-0.034\varepsilon + 0.099$ is obtained by fitting the strain-dependent energy difference of the two excitons (see Supporting

Information Figure S9). The linear coefficient of −0.034 or −34 meV/% is very close to the experimental value of −28 meV/% obtained from a similar fitting. From Figure 4d, we see that the experimental area ratio of P_2/P_4 increases dramatically with strain, and this is well modeled by the fit formula of eq 1, using the parameter values $a = 0.055$ and $b = 0.016$. The value of parameter a indicates the contribution of the direct transition in the overall linewidth. In this case, the ratio of radiative recombination inside the light cone over the total decay (sum of radiative recombination inside the light cone plus phonon-assisted recombination) is 0.055 at room temperature.

To have more quantitative measures of the strain effects on the PL qualities of bilayer $MoTe_2$, we compare the features of the PL spectrum of a strained bilayer $MoTe_2$ to those of typical unstrained monolayer and bilayer samples. As is shown in Figure 5a, the PL intensity of the strained bilayer has increased significantly and red-shifted compared to the unstrained one. The PL intensity becomes more comparable to that of the unstrained monolayer. An additional benefit is that the red-shifted emission of the strained bilayer $MoTe_2$ is further away from the silicon band edge (1.12 eV at room temperature, marked by a gray dashed line). This makes the strained bilayer material even more attractive than both the unstrained bilayer and the monolayer material for silicon-based devices due to the significantly reduced absorption. A more quantitative comparison of the relative PL yield can be found in Figure 5b. The PL yield (integrated intensity) of unstrained bilayer $MoTe_2$ in this work is 40% of that of the direct gap monolayer, comparable to the values extracted from refs 14 and 19. However, the relative PL yield reaches 70% of the monolayer material or a 1.75× increase under strain. In Figure 5c, the normalized PL spectra for the three cases are compared. The strained bilayer $MoTe_2$ has a spectral linewidth of 43.2 meV, much smaller than that of the unstrained bilayer (68.1 meV). The reduced linewidth is even smaller than that of the monolayer (48.6 meV). The strain-induced linewidth reduction is larger than that for other TMDCs[9−11] except for the bilayer WSe_2.[13] A detailed comparison can be found in the Supporting Information (see Figure S10). The linewidth contributions from various peaks are presented for the strained bilayer sample in Figure 5d. Although the linewidth of Peak 2 (the dominant exciton peak) is not significantly changed in the range of strain we studied, the overall linewidth is reduced by 36.6% as a result of changes of the relative contributions from various peaks by comparing with Figure 4d. As the strain is increased, the exciton contribution (P_2) to PL emission increases rapidly (Figure 4d), while contributions from other peaks either decrease (P_1) or remain the same (P_3). This leads to a dramatic reduction of the overall PL linewidth as seen in Figure 5c and 5d. As a result, the total linewidth of the PL spectrum eventually reflects the intrinsic linewidth of the neutral exciton emission at high levels of strain (compare for example 48.1 meV for the total linewidth vs 45.5 meV for the exciton linewidth at a strain level of 1.54%).

CONCLUSION

In summary, we have systematically studied the effects of mechanical strain on the photoluminescence properties of bilayer $MoTe_2$, both experimentally and theoretically. Our results demonstrate a clear trend of indirect to direct bandgap within a reasonably low level of strain. The significant improvement of PL properties as reflected by the increased PL intensity and reduced linewidth demonstrates the effectiveness of strain engineering, especially on bilayer $MoTe_2$, due to a relatively small difference between the indirect and direct bandgaps in $MoTe_2$ compared to other bilayer TMDCs. Our detailed theory-experiment comparison also allowed us to explain the mechanism of PL intensity increase and the reduction of the PL linewidth. We found that strain plays the role of purifying the emission processes, making the intrinsic exciton emission the eventual dominant mechanism, leading to the enhanced emission and a reduced linewidth that is comparable to that of its monolayer counterpart. We believe that our method of study and the mechanisms identified could apply to other TMDC materials. From the application point of view, a strained bilayer is more preferable to both the unstrained bilayer and the monolayer counterparts, due to the significant red-shift of the PL peak relative to the silicon absorption edge, making strained bilayer $MoTe_2$ one of the few 2D layered materials suitable for silicon-based photonic applications.

METHODS

Experimental Section. To prepare the samples, Scotch tape (3 M 810-12BX-CA) was used to exfoliate $MoTe_2$ flakes from bulk material (2D Semiconductors). The tapes were then pressed against polydimethylsiloxane (PDMS) (Dow Corning SYLGARD 184) films and slowly peeled off to transfer the flakes to PDMS. The stiffness of the PDMS was determined by the volume ratio between the base and the cure agent. Typically a 10:1 ratio is used. But for a higher efficiency of strain transfer, a more rigid PDMS is favorable.[39] Thus, a 5:1 ratio was used instead. The solution was cured in air at room temperature for 48 h after the mixture was formed. Bilayer $MoTe_2$ samples on PDMS were identified by their optical contrasts and subsequent PL measurements. Micro-PL measurements were conducted on a home-built system. A continuous-wave 633 nm He-Ne laser was used as the excitation source. The incident laser was focused by a 50× NIR objective (Mitutoyo) with a spot size of around 2 μm. In the strain-dependent PL measurement, the laser was refocused every time a different level of strain was applied, as the height of the sample had changed. The PL signal was collected by an InGaAs detector (Symphony) coupled to the monochromator (Horiba iHR 320). The PDMS films were then cut into pieces of 1 cm × 2 cm × 0.5 cm with bilayer $MoTe_2$ located at the center of each piece. The uniform geometry allows consistent strain control among different samples. The sample was then covered with another thin layer of PDMS deposited by drop-casting. The top layer of PDMS is around 10−20 μm thick. It serves to clamp the 2D material, enabling larger strain to be transferred to it from the bent PDMS. In our experiments we found the differences brought by the capping layer to be significant as described in more detail in Section 9 of the Supporting Information.

We would also like to point out the possible overestimation in the values of the strain in this work. Previous studies indicate weak adhesion between the TMDC and the substrate,[40] and the maximum strain applied to a monolayer on a single sided PDMS was estimated to be around 0.2%.[41] However, by considering the specific structure of samples in our experiment and the estimated exciton shift rate compared with previous studies, we determine the lower limit of the "actual" value of maximum strain to be 0.8%. Detailed discussion on the possible error of the estimated strain values can be found in Section 9 of the Supporting Information.

In the temperature-dependent PL measurement, a 10× objective was used to focus the pump laser and to collect the signal. Bilayer $MoTe_2$ samples on PDMS were put into a cryostat (Janis ST-500) cooled by flowing liquid nitrogen with a temperature controller (LakeShore model 331). The maximum actual laser power at the $MoTe_2$ plane was around 5 mW. No sample damage was observed at such a power level.

Theoretical Calculations. Band structure calculation of the bilayer $MoTe_2$ was performed by using the DFT+GW scheme as implemented in the VASP software package.[42] Given the ambient experimental condition in the present work, only the 2H phase (with hexagonal 2D lattice) for unstrained $MoTe_2$ was considered. The geometry optimization calculations used a plane-wave basis set with energy cutoff 400 eV and optB86b functional,[43] which includes a nonlocal correction for van der Waals interaction. The lattice constant of the 2D hexagonal lattice used in the DFT+GW calculation was $a = 3.467$ Å, which was obtained by the DFT level optimization with the settings listed above. A unit cell with $c = 28$ Å was used in conjunction with a 10 × 10 × 1 k-point mesh to ensure the vacuum separation between periodical images. No symmetry constraints were applied in the calculations. The uniaxial strain was simulated by distortion of the unit cell in the $a + b$ direction. We noted that qualitatively very similar results were obtained with distortion in the $a - b$ direction.

Using the optimized geometries, the quasi-particle band structures of $MoTe_2$ were calculated at the G_0W_0 level. To this end, the initial wave functions incorporating 120 energy bands are calculated by using the hybrid functional HSE06[44] with SOC interaction included. After the G_0W_0 step, the band structures were interpolated by using the Wannier90 postprocess package.[45] The GW calculations were tested by using 120 bands and 160 bands, respectively. At zero strain, the calculations by using both settings converged smoothly. The band structures obtained from both settings agree well with each other as well as with previous calculations.[14] For the strained lattices, we used a modified k-point path to sample the Brillouin zone with reduced symmetry and therefore reflect the lifted degeneracy (see Supporting Information Figure S2).

The exciton binding energy is obtained from the solution of the Wannier equation (similar to the Bethe−Salpeter equation) with hyperbolic bands, where the parameters of the bands are taken from approximate fits of the DFT-GW band structure (see Supporting Information Figure S7).

ASSOCIATED CONTENT

Supporting Information

The Supporting Information is available free of charge at https://pubs.acs.org/doi/10.1021/acsnano.2c01665.

> Fitting of the temperature- and pumping-dependent PL spectra at 77K; k-point selection in plotting the band structures under strained conditions; electronic band structures for bilayer $MoTe_2$ using DFT+GW calculations; fitting of the strain-dependent PL spectra at room temperature; estimation of the exciton binding energy; theory−experiment comparison on the area ratio P_1/P_2; estimated exciton energy difference ΔE; linewidth reduction comparison between different TMDCs under strain; strain transfer efficiency between PDMS and $MoTe_2$. (PDF)

AUTHOR INFORMATION

Corresponding Authors

Cun-Zheng Ning − *School of Electrical, Energy, and Computer Engineering, Arizona State University, Tempe, Arizona 85287, United States;* Present Address: (C.-Z.N.) Department of Electronic Engineering and Tsinghua International Center for Nano-Optoelectronics, Tsinghua University, Beijing 100084, China; Email: cning@asu.edu, cning@tsinghua.edu.cn

Rolf Binder − *Wyant College of Optical Sciences, University of Arizona, Tucson, Arizona 85721, United States;* Email: binder@optics.arizona.edu

Stefan Schumacher − *Department of Physics and Center for Optoelectronics and Photonics Paderborn (CeOPP), Paderborn University, Paderborn 33098, Germany; Wyant College of Optical Sciences, University of Arizona, Tucson, Arizona 85721, United States;* orcid.org/0000-0003-4042-4951; Email: stefan.schumacher@uni-paderborn.de

Authors

Yueyang Yu − *School of Electrical, Energy, and Computer Engineering, Arizona State University, Tempe, Arizona 85287, United States;* orcid.org/0000-0001-8771-0811

Chuan-Ding Dong − *Department of Physics and Center for Optoelectronics and Photonics Paderborn (CeOPP), Paderborn University, Paderborn 33098, Germany;* orcid.org/0000-0001-8438-4416

Complete contact information is available at: https://pubs.acs.org/10.1021/acsnano.2c01665

Notes

The authors declare no competing financial interest.

ACKNOWLEDGMENTS

We gratefully acknowledge the use of facilities at the Eyring Materials Center at Arizona State University and support by the U.S. National Science Foundation (NSF) under grant No. ECCS-1807644 (ASU group) and DMR 1839570 (U of A group). The Paderborn group acknowledges funding from the Deutsche Forschungsgemeinschaft through project SCHU∼1980/13 and the Heisenberg program (No.∼270619725). Grants for computing time at the Paderborn Center for Parallel Computing and High Performance Computing (HPC) at the University of Arizona are also gratefully acknowledged.

REFERENCES

(1) Xia, F.; Wang, H.; Xiao, D.; Dubey, M.; Ramasubramaniam, A. Two-Dimensional Material Nanophotonics. *Nat. Photonics* **2014**, *8*, 899−907.

(2) Li, Y.; Sun, H.; Gan, L.; Zhang, J.; Feng, J.; Zhang, D.; Ning, C.-Z. Optical Properties and Light-Emission Device Applications of 2-D Layered Semiconductors. *Proc. IEEE* **2020**, *108*, 676−703.

(3) Zhang, L.; Zunger, A. Evolution of Electronic Structure as a Function of Layer Thickness in Group-VIB Transition Metal Dichalcogenides: Emergence of Localization Prototypes. *Nano Lett.* **2015**, *15*, 949−957.

(4) Kumar, A.; Ahluwalia, P. K. Electronic Structure of Transition Metal Dichalcogenides Monolayers 1H-MX_2 (M = Mo, W; X = S, Se, Te) from Ab-Initio Theory: New Direct Band Gap Semiconductors. *Eur. Phys. J. B* **2012**, *85*, 1−7.

(5) Lloyd, D.; Liu, X.; Christopher, J. W.; Cantley, L.; Wadehra, A.; Kim, B. L.; Goldberg, B. B.; Swan, A. K.; Bunch, J. S. Band Gap Engineering with Ultralarge Biaxial Strains in Suspended Monolayer MoS_2. *Nano Lett.* **2016**, *16*, 5836−5841.

(6) Conley, H. J.; Wang, B.; Ziegler, J. I.; Haglund, R. F., Jr; Pantelides, S. T.; Bolotin, K. I. Bandgap Engineering of Strained Monolayer and Bilayer MoS_2. *Nano Lett.* **2013**, *13*, 3626−3630.

(7) Blundo, E.; Felici, M.; Yildirim, T.; Pettinari, G.; Tedeschi, D.; Miriametro, A.; Liu, B.; Ma, W.; Lu, Y.; Polimeni, A. Evidence of the Direct-to-Indirect Band Gap Transition in Strained Two-Dimensional WS_2, MoS_2, and WSe_2. *Physical Review Research* **2020**, 2, 012024.

(8) Island, J. O.; Kuc, A.; Diependaal, E. H.; Bratschitsch, R.; van der Zant, H. S. J.; Heine, T.; Castellanos-Gomez, A. Precise and Reversible Band Gap Tuning in Single-Layer $MoSe_2$ by Uniaxial Strain. *Nanoscale* **2016**, *8*, 2589−2593.

(9) Aslan, O. B.; Datye, I. M.; Mleczko, M. J.; Sze Cheung, K.; Krylyuk, S.; Bruma, A.; Kalish, I.; Davydov, A. V.; Pop, E.; Heinz, T. F. Probing the Optical Properties and Strain-Tuning of Ultrathin $Mo_{1-x}W_xTe_2$. *Nano Lett.* **2018**, *18*, 2485−2491.

(10) Niehues, I.; Schmidt, R.; Drüppel, M.; Marauhn, P.; Christiansen, D.; Selig, M.; Berghäuser, G.; Wigger, D.; Schneider, R.; Braasch, L.; et al. Strain Control of Exciton−Phonon Coupling in Atomically Thin Semiconductors. *Nano Lett.* **2018**, *18*, 1751−1757.

(11) Aslan, O. B.; Deng, M.; Heinz, T. F. Strain Tuning of Excitons in Monolayer WSe_2. *Phys. Rev. B* **2018**, *98*, 115308.

(12) Wang, Y.; Cong, C.; Yang, W.; Shang, J.; Peimyoo, N.; Chen, Y.; Kang, J.; Wang, J.; Huang, W.; Yu, T. Strain-Induced Direct−indirect Bandgap Transition and Phonon Modulation in Monolayer WS_2. *Nano Research* **2015**, *8*, 2562−2572.

(13) Desai, S. B.; Seol, G.; Kang, J. S.; Fang, H.; Battaglia, C.; Kapadia, R.; Ager, J. W.; Guo, J.; Javey, A. Strain-Induced Indirect to Direct Bandgap Transition in Multilayer WSe_2. *Nano Lett.* **2014**, *14*, 4592−4597.

(14) Robert, C.; Picard, R.; Lagarde, D.; Wang, G.; Echeverry, J. P.; Cadiz, F.; Renucci, P.; Högele, A.; Amand, T.; Marie, X.; et al. Excitonic Properties of Semiconducting Monolayer and Bilayer $MoTe_2$. *Phys. Rev. B* **2016**, *94*, 155425.

(15) Mak, K. F.; Lee, C.; Hone, J.; Shan, J.; Heinz, T. F. Atomically Thin MoS_2: A New Direct-Gap Semiconductor. *Phys. Rev. Lett.* **2010**, *105*, 136805.

(16) He, J.; Hummer, K.; Franchini, C. Stacking Effects on the Electronic and Optical Properties of Bilayer Transition Metal dichalcogenides MoS_2,$MoSe_2$,WS_2, andWSe_2. *Phys. Rev. B Condens. Matter Mater. Phys.* **2014**, *89*, 075409.

(17) Kuc, A.; Zibouche, N.; Heine, T. Influence of Quantum Confinement on the Electronic Structure of the Transition Metal Sulfide TS_2. *Phys. Rev. B Condens. Matter Mater. Phys.* **2011**, *83*, 245213.

(18) Sun, Y.; Wang, D.; Shuai, Z. Indirect-to-Direct Band Gap Crossover in Few-Layer Transition Metal Dichalcogenides: A Theoretical Prediction. *J. Phys. Chem. C* **2016**, *120*, 21866−21870.

(19) Froehlicher, G.; Lorchat, E.; Berciaud, S. Direct versus Indirect Band Gap Emission and Exciton-Exciton Annihilation in Atomically Thin Molybdenum Ditelluride ($MoTe_2$). *Phys. Rev. B Condens. Matter* **2016**, *94*, 085429.

(20) Lezama, I. G.; Arora, A.; Ubaldini, A.; Barreteau, C.; Giannini, E.; Potemski, M.; Morpurgo, A. F. Indirect-to-Direct Band Gap Crossover in Few-Layer $MoTe_2$. *Nano Lett.* **2015**, *15*, 2336−2342.

(21) Helmrich, S.; Schneider, R.; Achtstein, A. W.; Arora, A.; Herzog, B.; de Vasconcellos, S. M.; Kolarczik, M.; Schöps, O.; Bratschitsch, R.; Woggon, U.; et al. Exciton−phonon Coupling in Mono- and Bilayer $MoTe_2$. *2D Mater.* **2018**, *5*, 045007.

(22) Ravindra, N. M.; Srivastava, V. K. Temperature Dependence of the Energy Gap in Semiconductors. *J. Phys. Chem. Solids* **1979**, *40*, 791−793.

(23) Sie, E. J.; Steinhoff, A.; Gies, C.; Lui, C. H.; Ma, Q.; Rösner, M.; Schönhoff, G.; Jahnke, F.; Wehling, T. O.; Lee, Y.-H.; et al. Observation of Exciton Redshift−Blueshift Crossover in Monolayer WS_2. *Nano Lett.* **2017**, *17*, 4210−4216.

(24) Ruppert, C.; Aslan, O. B.; Heinz, T. F. Optical Properties and Band Gap of Single- and Few-Layer $MoTe_2$ Crystals. *Nano Lett.* **2014**, *14*, 6231−6236.

(25) Yang, J.; Lü, T.; Myint, Y. W.; Pei, J.; Macdonald, D.; Zheng, J.-C.; Lu, Y. Robust Excitons and Trions in Monolayer $MoTe_2$. *ACS Nano* **2015**, *9*, 6603−6609.

(26) Brem, S.; Ekman, A.; Christiansen, D.; Katsch, F.; Selig, M.; Robert, C.; Marie, X.; Urbaszek, B.; Knorr, A.; Malic, E. Phonon-Assisted Photoluminescence from Indirect Excitons in Monolayers of Transition-Metal Dichalcogenides. *Nano Lett.* **2020**, *20*, 2849−2856.

(27) Yun, W. S.; Han, S. W.; Hong, S. C.; Kim, I. G.; Lee, J. D. Thickness and Strain Effects on Electronic Structures of Transition Metal Dichalcogenides: 2H-MX2semiconductors (M = Mo, W;X = S, Se, Te). *Phys. Rev. B Condens. Matter Mater. Phys.* **2012**, *85*, 033305.

(28) Niehues, I.; Marauhn, P.; Deilmann, T.; Wigger, D.; Schmidt, R.; Arora, A.; Michaelis de Vasconcellos, S.; Rohlfing, M.; Bratschitsch, R. Strain Tuning of the Stokes Shift in Atomically Thin Semiconductors. *Nanoscale* **2020**, *12*, 20786−20796.

(29) Cui, H.-J.; Sheng, X.-L.; Yan, Q.-B.; Zheng, Q.-R.; Su, G. Strain-Induced Dirac Cone-like Electronic Structures and Semiconductor−semimetal Transition in Graphdiyne. *Phys. Chem. Chem. Phys.* **2013**, *15*, 8179−8185.

(30) Jones, A. M.; Yu, H.; Ross, J. S.; Klement, P.; Ghimire, N. J.; Yan, J.; Mandrus, D. G.; Yao, W.; Xu, X. Spin−layer Locking Effects in Optical Orientation of Exciton Spin in Bilayer WSe_2. *Nat. Phys.* **2014**, *10*, 130−134.

(31) Gerber, I.; Courtade, E.; Shree, S.; Robert, C.; Marie, X.; Watanabe, K.; Taniguchi, T.; Urbaszek, B. Interlayer Excitons in Bilayer MoS_2 with Strong Oscillator Strength up to Room Temperature. *Phys. Rev. B* **2019**, *99*, 035443.

(32) Carrascoso, F.; Lin, D.-Y.; Frisenda, R.; Castellanos-Gomez, A. Biaxial Strain Tuning of Interlayer Excitons in Bilayer MoS_2. *J. Phys. Mater.* **2020**, *3*, 015003.

(33) Niehues, I.; Blob, A.; Stiehm, T.; de Vasconcellos, S. M.; Bratschitsch, R. Interlayer Excitons in Bilayer MoS_2 under Uniaxial Tensile Strain. *Nanoscale* **2019**, *11*, 12788−12792.

(34) Horng, J.; Stroucken, T.; Zhang, L.; Paik, E. Y.; Deng, H.; Koch, S. W. Observation of Interlayer Excitons in $MoSe_2$ Single Crystals. *Phys. Rev. B* **2018**, *97*, 241404.

(35) Wang, Z.; Chiu, Y.-H.; Honz, K.; Mak, K. F.; Shan, J. Electrical Tuning of Interlayer Exciton Gases in WSe_2 Bilayers. *Nano Lett.* **2018**, *18*, 137−143.

(36) Miller, B.; Steinhoff, A.; Pano, B.; Klein, J.; Jahnke, F.; Holleitner, A.; Wurstbauer, U. Long-Lived Direct and Indirect Interlayer Excitons in van Der Waals Heterostructures. *Nano Lett.* **2017**, *17*, 5229−5237.

(37) Sigl, L.; Troue, M.; Katzer, M.; Selig, M.; Sigger, F.; Kiemle, J.; Brotons-Gisbert, M.; Watanabe, K.; Taniguchi, T.; Gerardot, B. D.; et al. Optical Dipole Orientation of Interlayer Excitons in $MoSe_2$−WSe_2 Heterostacks. *Phys. Rev. B Condens. Matter* **2022**, *105*, DOI: 10.1103/PhysRevB.105.035417.

(38) Lindlau, J.; Selig, M.; Neumann, A.; Colombier, L.; Förste, J.; Funk, V.; Förg, M.; Kim, J.; Berghäuser, G.; Taniguchi, T.; et al. The Role of Momentum-Dark Excitons in the Elementary Optical Response of Bilayer WSe_2. *Nat. Commun.* **2018**, *9*, 1−7.

(39) Guo, G.; Zhu, Y. Cohesive-Shear-Lag Modeling of Interfacial Stress Transfer Between a Monolayer Graphene and a Polymer Substrate. *J. Appl. Mech.* **2015**, *82*, 031005.

(40) Rokni, H.; Lu, W. Direct Measurements of Interfacial Adhesion in 2D Materials and van Der Waals Heterostructures in Ambient Air. *Nat. Commun.* **2020**, *11*, 5607.

(41) Plechinger, G.; Castellanos-Gomez, A.; Buscema, M.; van der Zant, H. S. J.; Steele, G. A.; Kuc, A.; Heine, T.; Schüller, C.; Korn, T. Control of Biaxial Strain in Single-Layer Molybdenite Using Local Thermal Expansion of the Substrate. *2D Mater.* **2015**, *2*, 015006.

(42) Kresse, G.; Furthmüller, J. Efficiency of Ab-Initio Total Energy Calculations for Metals and Semiconductors Using a Plane-Wave Basis Set. *Comput. Mater. Sci.* **1996**, *6*, 15−50.

(43) Klimeš, J.; Bowler, D. R.; Michaelides, A. Chemical Accuracy for the van Der Waals Density Functional. *J. Phys.: Condens. Matter* **2010**, *22*, 022201.

(44) Krukau, A. V.; Vydrov, O. A.; Izmaylov, A. F.; Scuseria, G. E. Influence of the Exchange Screening Parameter on the Performance of Screened Hybrid Functionals. *J. Chem. Phys.* **2006**, *125*, 224106.

(45) Mostofi, A. A.; Yates, J. R.; Lee, Y.-S.; Souza, I.; Vanderbilt, D.; Marzari, N. wannier90: A Tool for Obtaining Maximally-Localised Wannier Functions. *Comput. Phys. Commun.* **2008**, *178*, 685−699.